# PdAu/C catalysts prepared by plasma sputtering for the electro-oxidation of glycerol

Mathieu Mougenot, Amaël Caillard, Mario Simoes, Steve Baranton, Christophe Coutanceau, Pascal Brault

# PdAu/C catalysts prepared by plasma sputtering for the electro-oxidation of glycerol

**M. Mougenot[1], A. Caillard[1], M. Simoes[2], S. Baranton[2], C. Coutanceau[2], P. Brault[1]**

[1] Groupe de Recherche sur l'Energétique des Milieux Ionisés (GREMI), UMR6606, CNRS-Université d'Orléans, 14 rue d'Issoudun, BP6744, 45067 ORLEANS Cedex 2, France.

[2] Laboratoire de Catalyse en Chimie Organique (LACCO), e-lyse, UMR6503, CNRS-Université de Poitiers, 40 avenue du Recteur Pineau, 86022 Poitiers, France.

Corresponding authors: Pascal.Brault@univ-orleans.fr and Christophe.Coutanceau@univ-poitiers.fr

**Abstract**

*Co-sputtered $Pd_{0.7}Au_{0.3}$ catalyst and alternate sputtered $Pd_{0.35}Au_{0.3}Pd_{0.35}$ and $Au_{0.15}Pd_{0.7}Au_{0.15}$ materials were prepared by plasma deposition of Au and Pd atoms on a carbon diffusion layer. Atomic composition and metal loadings were evaluated from EDX and RBS, respectively. The low amount of deposited and of the resulting low metallic film thickness made TEM and XRD characterizations difficult to perform, therefore, catalyst microstructures and surface compositions were determined from electrochemical methods and compared with data obtained with Pd/C, Au/C and $Pd_{0.7}Au_{0.3}$/C materials synthesized via the water in oil microemulsion method. The surface of co-sputtered $Pd_{0.7}Au_{0.3}$ and alternate sputtered $Pd_{0.35}Au_{0.3}Pd_{0.35}$ and $Au_{0.15}Pd_{0.7}Au_{0.35}$ materials are partly composed by PdAu alloy. The plasma sputtering method leads to more active bimetallic PdAu material than the wet chemistry method. Modification of palladium surface by gold atoms leads to increase the catalytic activity toward glycerol electrooxidation. The PdAu surface alloy composition has no significant effect on the catalytic activity, however, the presence of non-alloyed gold sites on the material surface leads to the enhancement of the catalytic activity. The mechanism seems to involve glycerol adsorption on palladium surface and hydroxyl species formation on gold surface leading to catalytic activity enhancement through the bifunctional mechanism.*

**Keywords:** Alloys, DGFC, Gold, Palladium, Glycerol, Electrooxidation, Plasma sputtering.

## 1. Introduction

The study of alcohol electro-oxidation is an important research domain because of its implication in fuel cell development and electro-synthesis. Moreover, the concept of cogeneration of electrical energy and added value chemicals has recently been proposed [1]. For this purpose, fuels cells could provide a profitable solution for valorising glycerol which is a by-product issued from the biodiesel industry. The increasing world production of methyl esters as fuel additive and of bioethanol leads to an increase of the glycerol production [2,3,4], making glycerol a cheap raw material from chemistry, so that it can be considered now as a secondary primary energy source. Glycerol has a theoretical energy density of 5.0 kWh $kg^{-1}$ and is less toxic than methanol which holds 6.1 kWh $kg^{-1}$ [5,6]. In a Solid Alkaline Membrane Fuel Cells (SAMFCs), its oxidation leading to $CO_3^{2-}$ formation involves the exchange of 14 moles of electrons per mole of glycerol according to Eq. 1:

$$CH_2OH\text{-}CHOH\text{-}CH_2OH + 20\ OH^- \rightarrow 3\ CO_3^{2-} + 14\ H_2O + 14\ e^- \quad (1)$$

However, such a SAMFC system could be profitable only if high electrical efficiency platinum-free electrodes and suitable catalytic orientation of the reaction path for cogenerating value-added compounds are achieved. In other words, high catalytic activity and high selectivity toward highly oxygenated compounds such as hydroxypyruvate (exchange of 6 moles of electrons per mole of glycerol according to Eq. 2), or mesoxalate (which involves the exchange of 10 moles of electrons per mole of glycerol according to Eq. 3) are targeted:

$$CH_2OH\text{-}CHOH\text{-}CH_2OH + 7\ OH^- \rightarrow CH_2OH\text{-}CO\text{-}COO^- + 6\ H_2O + 6\ e^- \quad (2)$$

$$CH_2OH\text{-}CHOH\text{-}CH_2OH + 12\ OH^- \rightarrow {}^-OOC\text{-}CO\text{-}COO^- + 10\ H_2O + 10\ e^- \quad (3)$$

allowing reaching 43 % and 71.5% of the theoretical energy density, respectively.

Palladium is an effective catalytic material for the oxidation of alcohols and polyols in alkaline medium [7,8]. Gold nanoparticles display also a catalytic activity toward alcohol oxidation due to their ability to form adsorbed AuOH species in alkaline medium [9]. This

material is efficient for hydroxypyruvate formation. It has recently been shown that bimetallic palladium-gold catalysts displayed a higher catalytic activity toward glycerol electrooxidation than monometallic materials, close to that of platinum [1]. Such synergetic effect between both metals is not still completely understood, and further studies with different PdAu catalyst structures may help to bring new insights.

Plasma deposition techniques are very convenient for the preparation of supported bimetallic catalysts [10,11]. Such techniques allow depositing very small quantities of material, changing the nanostructure (clusters, thin films, alloys, multilayers, etc.) [12,13,8] and optimizing the composition of the catalysts only by varying deposition parameters (co-sputtering, alternated sputtering, applied power, target voltage, etc.). Hence, these physical deposition methods are now largely used in the industry and in research for the fabrication of fuel cell catalytic layers [14,15,16,17]. In the present paper, Pd, Au, and different PdAu (in terms of atomic composition and structure) nanostructured catalytic layers were synthesized by plasma sputtering of metals on a gas diffusion layer. Their activity toward glycerol oxidation was characterized by cyclic voltammetry. These electrocatalysts were compared to a $Pd_{0.7}Au_{0.3}$/C catalyst issued from a wet chemistry synthesis method, namely the "water-in-oil" micro-emulsion method. An attempt to correlate the catalytic activity of the catalysts to their structural characterization data was made in order to gives some new insights on the "synergetic effect" between both metals.

## 2. Experimental

### 2.1. Catalyst preparation

A cylindrical stainless steel low pressure TCP sputtering reactor (260 mm height, 210 mm diameter) was used for the alternate deposition or the co-deposition of pure palladium and pure gold (both 99.999 % from Neyco). Both 2-inch metal targets, positioned at middle height, were 45° tilted in front of a plane rotating substrate holder. An argon plasma was created in the chamber by an external planar RF antenna (13.56 MHz) positioned on the top

glass window. The plasma chamber has been previously detailed for dual deposition [10]. Three series of experiments consisting in different sputtering configurations were performed (Table 1). The first one corresponded to single metal depositions (Pd and Au) for obtaining monometallic catalysts; the second one consisted in a simultaneous deposition of Au and Pd ($Pd_{0.7}Au_{0.3}$); the third one corresponded to alternate depositions of Au and Pd (three-layer catalysts) keeping a 7/3 Pd/Au atomic ratio ($Pd_{0.35}Au_{0.3}Pd_{0.35}$ and $Au_{0.15}Pd_{0.7}Au_{0.15}$). For Pd and Au co-deposition, the voltage applied to the two targets was independently adjusted in order to obtain the desired atomic composition in catalysts. For the three-layer catalysts, a voltage of -250 V was applied alternatively to both targets. The deposition time was modulated in order to obtain desired atomic compositions. All catalysts were deposited on a gas diffusion layer (ELAT® Gas Diffusion Layers, GDL, LT 1200-W, from Electrochem. Inc.). This sputtering technique allows depositing most of the atoms within the first 300 nm of the GDL.

Wet chemistry catalysts (w/t) were synthesized using the water in oil microemulsion method [1,18,19]. Briefly, catalysts were prepared by mixing $NaBH_4$ (99% from Acros Organics) as reducing agent, with a microemulsion carrying the specific reactants dissolved in an aqueous phase (Milli-Q Millipore, 18.2 MΩ cm). In particular, $K_2PdCl_4$ and $HAuCl_4 \cdot 3H_2O$ (from Alfa Aesar, 99.9%) were used. Poly(ethylene glycol)-dodecyl ether (BRIJ® 30 from Fluka) was chosen as surfactant, and the organic phase was *n*-heptane (99% from Acros Organics). The desired amount of metal salts was dissolved in ultrapure water in order to obtain metallic nanoparticles with controlled compositions after the reduction process with $NaBH_4$. Carbon (Vulcan XC72), previously treated under $N_2$ at 400°C for 4 h, was added directly in the colloidal solution to obtain the desired metal loading, and the mixture was kept under stirring for 2 h. In the present work all the catalysts were synthesized in order to obtain 40 wt % metal loading. The mixture was filtered on a 0.22 $\mu$m Durapore membrane filter (Millipore). The

resulting powder was abundantly rinsed with ethanol, acetone, and ultrapure water. The carbon-supported catalysts were dried overnight in an oven at 75 °C.

### 2.2. Catalyst characterization

Wet chemistry catalysts were characterized by Transmission Electron Microscopy (TEM) using a JEOL 2100 UHR microscope (200 kV) equipped with a $LaB_6$ filament. Images were taken with a camera Gatan Ultrascan 2k x 2k. The mean particle size and size distribution were determined by measuring the diameter of isolated particles using ImageJ free software, although particle agglomeration is present. Between 200 and 300 particles were considered for each catalyst in order to have an acceptable statistical sample. For the sputtered electrodes SEM micrographes were recorded in order to evaluate the layer morphologies. Rutherford Backscattering Spectroscopy (Van de Graaf accelerator, 2MeV $\alpha$ particle beam) used to measure the total metal loadings. For a better accuracy, the bulk composition was measured either by EDX (for sputtered electrodes) or ICP-OES (for chemically prepared catalysts). Surface composition, oxidation states and possible electronic interactions between metals were evaluated by X-ray Photoelectron Spectroscopy (XPS). Spectra were collected using a VG ESCALAB 3 MKII spectrometer using Mg $K_\alpha$ a monochromatic radiation (1253.6 eV). The source was operated at 300 W (15 kV and 20 mA). Powder analysis covered a surface of 2 mm x 3 mm.

### 2.3 Electrochemical measurements

In the case of wet chemistry catalyst, catalytic powder is deposited on a glassy carbon substrate according to a method proposed by Gloaguen et al. [20]. The catalytic powder (25 mg) was added to a mixture of 0.5 mL Nafion solution (5 wt% from Aldrich) in ultra-pure water (Millipore MilliQ, 12 MΩ cm). After ultrasonic homogenization of the catalyst/XC72-Nafion ink, a given volume was deposited from a syringe onto a fresh polished glassy carbon (0.071 $cm^2$ geometric surface area) substrate yielding a catalytic powder loading of 354 µg

$cm^{-2}$, i.e. 142 µg $cm^{-2}$ metal loading. The solvent was then evaporated in a stream of ultra-pure nitrogen at room temperature. By this way, a catalytic layer was obtained with a thickness of about 1µm [19].

In the case of sputtered electrodes, a pre-cut disc of electrode is pressed against a glassy carbon disc inserted in a PTFE cylindrical holder and blocked using a cap with a hole of 4 mm diameter. The electrode surface is then 0.126 $cm^2$.

The electrochemical set-up consisted in a Voltalab PGZ 402 computer controlled potentiostat. The electrochemical experiments were carried out at 20 °C in $N_2$-purged supporting electrolyte, using a conventional thermostated three-electrode electrochemical cell. The counter electrode was a glassy carbon plate (8 $cm^2$ geometric surface area) and the reference electrode was a Reversible Hydrogen Electrode (RHE). Cyclic voltammetry were recorded at v = 50 mV $s^{-1}$, in $N_2$-saturated 1.0 M NaOH (Semiconductor Grade 99.99%, Sigma–Aldrich) in ultra-pure water supporting electrolyte. Their activity toward the glycerol electro-oxidation was characterised by recording the polarisation curves j(E) under the following experimental conditions: 1.0 M NaOH + 0.1 M Glycerol (Reagent Plus 99%, Sigma–Aldrich), $N_2$-saturated, v = 10 mV $s^{-1}$.

## 3. Result and discussion

### 3.1. Catalyst characterization

The weight metal loadings of plasma sputtered electrodes were determined by Rutherford Backscattering Spectroscopy (RBS). RBS spectra recorded between 1500 and 2000 keV on the co-sputtered $Pd_{0.7}Au_{0.3}$, and the alternate sputtered $Pd_{0.35}Au_{0.3}Pd_{0.35}$ and $Au_{0.15}Pd_{0.7}Au_{0.15}$ materials are displayed in Figure 1. The co-sputtered $Pd_{0.7}Au_{0.3}$ displays two peaks, centred at 1710 and 1825 keV, corresponding to palladium and gold atoms, respectively. The shape of these 2 peaks is asymmetrical which is attributed to the penetration of atoms in the porous GDL. The area under each peak is directly related to the number of atoms inside the GDL.

Using the simnra® software, a bulk Pd/Au atomic ratio of 7/3 and a total metal loading of 66 µg/cm² were evaluated. The spectrum corresponding to the alternate $Pd_{0.35}Au_{0.3}Pd_{0.35}$ catalyst displays a double peak for palladium and a single peak for gold, whereas a single Pd peak and a double Au peak are observed for the $Au_{0.15}Pd_{0.7}Au_{0.15}$ catalyst. The total weight metal loadings were evaluated to be ca. 62 and ca. 72 µg $cm^{-2}$, respectively. The RBS spectra of both sputtered monometallic catalysts Pd and Au were also recorded (not shown here) and the corresponding weight metal loadings are reported in the Table 1. RBS spectra of pure Pd and Au sputtered layers allowed also to estimate the thickness of the sputtered layer. It was found that in both cases, 90 % of the metal atoms were deposited within 300 nm depth of the carbon GDL. This result is close to that obtained with Pt deposition using the same technique [21].

SEM images of the co-sputtered $Pd_{0.7}Au_{0.3}$ material and the alternate sputtered $Pd_{0.35}Au_{0.3}Pd_{0.35}$ catalyst, as an example, deposited on the GDL are presented in Figure 2a and Figure 2b, respectively. The change in metal deposition method (co- or alternate sputtering) doesn't affect the morphology of the electrode: both SEM images display catalyzed carbon nodules with a diameter in the range of ca. 50-100 nm. Table 1 summarizes the catalyst preparation method and the physicochemical characterization data recorded for all studied sputtered catalysts, i. e. the total weight composition (70 ± 8 µg $cm^{-2}$ of metal for all samples), and the atomic ratio as determined by EDX.

Figures 3 presents the cyclic voltammograms of sputtered monometallic catalysts recorded in deareated 0.1 M NaOH supporting electrolyte at a scan rate of 50 mV $s^{-1}$. Voltammograms of sputtered Pd and Au electrodes resemble typical voltammograms of clean catalytic nanoparticles supported on carbon recorded in an alkaline medium. Pd catalyst shows a clear and sharp reduction peak centered at ca. 0.62 V *vs* RHE as it was observed earlier for the Pd/C catalyst prepared via the water in oil colloidal method [18], whereas Au sample present a broader reduction peak centered at ca. 1.04 V *vs* RHE. For pure Pd catalysts,

voltammograms were recorded with the upper potential set at 1.45 V *vs* RHE, leading to the formation of a monolayer of palladium oxide [22]. Considering a charge density of 424 μC $cm^{-2}$ for the reduction of a PdO monolayer from a bulk Pd polycrystalline surface [18], the electrochemical surface areas of the pure palladium catalysts were estimated at ca. 36 $m^2$ $g^{-1}$ and ca. 28 $m^2$ $g^{-1}$; for sputtered Pd and wet chemistry Pd catalysts [18], respectively. For pure Au catalysts, voltammograms were recorded with the upper potential set at 1.55 V vs RHE in order to measure during the negative scan the reduction of a gold oxide layer [23]. Such upper potential limit is low enough to avoid the oxygen evolution reaction and high enough to allow better accuracy for the determination of the charge involved in the reduction peak. A charge density of 493 μC $cm^{-2}$ is associated to the reduction of an oxide layer on bulk polycrystalline gold surface when an upper potential limit is set at 1.55 V [25], whereas a value of 400 μC $cm^{-2}$ is proposed for the reduction of a AuOH monolayer when an upper potential limit is set at 1.45 V vs RHE [24,25]. Electrochemical surface areas of ca. 11 $m^2$ $g^{-1}$ and ca. 8 $m^2$ $g^{-1}$ were estimated for sputtered Au and wet chemistry Au [18] catalysts, respectively. From the electrochemical surface area and assuming a spherical shape and similar diameter (d) for the nanoparticles, the "electrochemical" mean particle size of Pd and Au catalysts expressed in nm can be estimated using the following equations [26]:

$$S_p = \pi d^2 \tag{4}$$

$$V_p = \frac{\pi d^3}{6} \tag{5}$$

$$S_{real} = \frac{S_p}{V_p \times \rho} = \frac{\pi d^2}{\frac{\pi d^3}{6} \times \rho} = \frac{6}{d \times \rho} \tag{6}$$

$$d_{EC}(nm) = \frac{6}{\rho\left(g\,nm^{-3}\right) \times ESA\left(nm^2\,g^{-1}\right)} = \frac{6000}{\rho\left(g\,cm^{-3}\right) \times ESA\left(m^2\,g^{-1}\right)} \tag{7}$$

where $S_p$ is particle surface, $V_p$ the particle volume, $\rho$ the density of metal ($\rho_{Pd}$ = 12.02 g cm$^{-3}$ and $\rho_{Au}$ = 19.32 g cm$^{-3}$) and ESA the electrochemical surface area (in m$^2$ g$^{-1}$). The following mean particle sizes were calculated: $d_{EC}^{Pd,sputt.}$ = 13.9 nm, $d_{EC}^{Pd,w/c}$ = 17.8 nm, $d_{EC}^{Au,sputt.}$ = 28.2 nm and $d_{EC}^{Au,w/c}$ = 38.8 nm. Because the electrochemical reactions involved for the determination of ESAs are surface oxidation/reduction, the related particles sizes calculated from ESA ($d_{EC}^{Pd,w/c}$ and $d_{EC}^{Au,w/c}$) were compared to the surface weighted mean particle sizes ($d_s$) determined from TEM measurement on Pd/C (Figure 4a) and a Au/C (Figure 4b) materials prepared from wet chemistry method. The following equation was used:

$$d_s = \frac{\sum_1^n n_i d_i^3}{\sum_1^n n_i d_i^2} \tag{8}$$

Surface weighted mean particle sizes ($d_s$) of ca. 4.3 and 8.3 were found for the wet chemistry Pd/C and Au/C catalysts, respectively. The ratio ($ESA_{Pd}/ESA_{Au}$) can be compared to the ratio involving the mean particle size as determined by TEM:

$$\frac{ESA_{Pd}}{ESA_{Au}} = \frac{\frac{6000}{\rho_{Pd} \times d_{EC}^{Pd}}}{\frac{6000}{\rho_{Au} \times d_{EC}^{Au}}} = \frac{\rho_{Au} \times d_s^{Au}}{\rho_{Pd} \times d_s^{Pd}} \tag{9}$$

$$\frac{ESA_{Pd}}{ESA_{Au}} = \frac{28}{8} = 3.5 \tag{10}$$

$$\frac{\rho_{Au} \times d_s^{Au}}{\rho_{Pd} \times d_s^{Pd}} = \frac{19.32 \times 8.3}{12.02 \times 4.3} = 3.1 \tag{11}$$

The relative error between both values, determined from equation 10 and equation 11, is below 15%, which indicates that electrochemical and TEM measurements are in good agreement, since the catalyst active surface area is related to the mean nanoparticle size. The

important difference between the particle size determined by electrochemical method and that determined by TEM can be explained by the fact that Au/C and Pd/C catalyst exhibits agglomerated particles, with size greater than 20 nm for gold catalyst (not shown), which were not taken into account for the determination of the mean particle size during TEM measurements. Moreover, the particle part in contact with the carbon support may not be involved in the surface reactions. This leads to a higher value of the active surface area calculated by TEM measurements for both Au/C and Pd/C catalysts, when compared to electrochemical methods.

The determination of particle size from TEM images of metal sputtered on a carbon diffusion layer is very difficult to obtain [10]. However, it is worth to remark that about same $ESA_{Pd}/ESA_{Au}$ ratio was obtained (ca. 3.27) with sputtered monometallic catalysts. Assuming that the agglomeration effect is the same for wet chemistry and sputtered monometallic catalysts, although the metal loading is twice lower on sputtered Pd and Au catalysts than on wet chemistry catalysts, surface weighted particles sizes of ca. 3.4 nm and ca. 5.8 nm were estimated. The assumption is supported by the fact that plasma sputtering of metal leads to relatively dense catalytic film located on the diffusion layer surface and shallowness [27]. It seems then that plasma sputtering process allows obtaining metal nanoparticles with smaller mean sizes than the wet chemical syntheses.

As catalytic reactions take place at the electrode surface, it is important to evaluate the surface structure of $Pd_xAu_{1-x}$ bimetallic materials. The surface structure of the $Pd_xAu_{1-x}$ catalysts was investigated by cyclic voltammetry recorded in supporting alkaline electrolyte. For this purpose, voltammograms of PdAu catalysts were performed with the upper potential limit set at 1.45 V *vs* RHE. Figure 5 displays the voltammetric cycles obtained for $Pd_{0.7}Au_{0.3}$ co-sputtered catalyst, and $Pd_{0.35}Au_{0.3}Pd_{0.35}$ and $Au_{0.15}Pd_{0.7}Au_{0.15}$ alternate sputtered catalysts. The voltammogram of co-sputtered $Pd_{0.7}Au_{0.3}$ material presents a small reduction peak at ca. 1.04

V related to non-alloyed gold sites at the material surface and a well marked broad oxide reduction peak located at ca. 0.70 V *vs* RHE in the negative scan, indicating that Pd-Au alloy is formed on the surface [28].The $Au_{0.15}Pd_{0.7}Au_{0.15}$ alternate sputtered catalyst also displays only an "alloy" peak at ca. 0.75 V and a gold peak at ca. 1.040 V. The $Pd_{0.35}Au_{0.3}Pd_{0.35}$ alternate sputtered catalyst displays two reduction peaks. The first one centered at ca. 0.62 V is related to oxide reduction of pure palladium sites, the second one is a shoulder centered at ca. 0.71 V (according to the first derivative of the j-E curve) related to oxide reduction of PdAu alloy sites; no oxide reduction peak ca. 1.04 V assigned to oxide reduction of gold sites is observed. According to Rand and woods [28], PdAu alloy catalyst surface composition can be determined from the palladium reduction peak position in the cyclic voltammograms recorded in supporting alkaline electrolyte. Table 1 displays bulk compositions of each catalyst measured by EDX and the alloy surface composition calculated according to the Rand and Wood method. Concerning the co-sputtered $Pd_{0.7}Au_{0.3}$, the alloy surface composition is a little bit palladium enriched, being ca. 80 at% of Pd and 20 at% of Au. This surface enrichment has been previously observed for $Pd_xAu_{1-x}$ materials synthesized by wet chemistry, e. g. the "water-in-oil" micro-emulsion method [18], but in a higher extent (ca. 88 at% Pd and 12 at% Au). The PdAu alloy surface is composed by ca. 77 at% of Pd and 23 at% of gold atoms in the $Pd_{0.35}Au_{0.3}Pd_{0.35}$ and of ca. 69 at% of Pd and ca. 31 at% of gold in $Au_{0.15}Pd_{0.7}Au_{0.15}$ material. The $Pd_{0.35}Au_{0.3}Pd_{0.35}$ catalyst displays a well marked reduction peak at ca. 0.62 V corresponding to the surface oxide reduction on pure palladium sites beside a shoulder coming from the oxide reduction of PdAu nanoalloy. No Pd oxide reduction peak is recorded on $Au_{0.15}Pd_{0.7}Au_{0.15}$ catalyst, which indicates that the surface is mainly composed of a PdAu alloy and non-alloyed gold sites.

The first important remark is that alternate pulverization of gold and palladium leads to the formation of surface PdAu alloys. The second one is that the surface alloy is palladium-rich in

comparison of global composition in the case of the co-sputtered catalyst. We now dispose of three samples with the same metal loading and global atomic composition but different surface compositions and structures. The surface of the co-sputtered $Pd_{0.7}Au_{0.3}$ catalyst is mainly formed by an alloy with an atomic ratio ca. $Pd_{0.80}Au_{0.20}$ and of isolated gold sites, the surface of the $Au_{0.15}Pd_{0.7}Au_{0.15}$ is composed of isolated gold sites (in higher amount than that for the co sputtered PdAu material as the reduction peak at ca. 1.04 has higher intensity) and of a surface alloy with a composition ca. $Pd_{0.69}Au_{0.31}$, and the surface of the $Pd_{0.35}Au_{0.3}Pd_{0.35}$ is formed of relatively high amount of palladium sites and a surface alloy with a composition ca. $Pd_{0.77}Au_{0.23}$.

From these results, an attempt was made to evaluate the electrochemical active surface area (or real surface area) by using a calculation method previously described [29]. Equations (12), (13) and (14) were used for the determination of the Pd real surface ($S_{Pd}$), Au real surface ($S_{Au}$) and PdAu alloy real surface ($S_{Pd\text{-}Au}$), respectively:

$$S_{Pd} = \frac{Q_{red}^{PdO}}{(\theta_{PdO} \times Q_{red,ML}^{PdO})} \quad (12)$$

$$S_{Au} = \frac{Q_{red}^{AuO}}{(\theta_{AuO} \times Q_{red,ML}^{AuO})} \quad (13)$$

$$S_{Pd-Au} = \frac{Q_{red}^{Pd-Au(O)}}{(\theta_{PdO} \times Q_{red,ML}^{PdO} \times X_{Pd} + \theta_{AuO} \times Q_{red,ML}^{AuO} \times X_{Au})} \quad (14)$$

where, $Q_{red}^{PdO}$, $Q_{red}^{AuO}$ and $Q_{red}^{Pd-Au(O)}$ are the charges involved in the reduction peak of Pd, Au and PdAu alloy, respectively; $\theta_{PdO}$ and $\theta_{AuO}$ are the surface coverage of metal by oxygen species, which are equal to 1 in the present experimental conditions considering the charge density involved for the reduction of an oxide monolayer on Pd ($Q_{red,ML}^{PdO}$) equal to 424 µC $cm^{-2}$ and that on Au ($Q_{red,ML}^{AuO}$) equal to 400 µC $cm^{-2}$. At last, $X_{Pd}$ and $X_{Au}$ represent the

atomic surface composition of the Pd/Au surface alloy as determined before using the Rand and Wood method. Table 2 summarizes the results obtained for the different bimetallic catalysts.

### 3.2. Electroactivity toward the glycerol electrooxidation reaction

The catalyst activity of the different PdAu catalysts toward the glycerol electro-oxidation was examined by cyclic voltammetry in the presence of 0.1 M glycerol. For the comparison of the electrochemical behavior of the different electrodes, the voltammograms were presented in terms of current density (Figures 6a,c) and in terms of activity related to the real surface area (Figures 6b,d). First, sputtered Au and Pd monometallic material, $Pd_{0.7}Au_{0.3}$/C catalysts prepared by co-sputtered and wet chemistry are compared in terms of activity toward the glycerol electrooxydation in Figure 6a,b. Glycerol electro-oxidation starts at same potential on pure Au catalyst as on pure Pd, but Pd catalyst leads very soon to higher reaction kinetics for glycerol oxidation than the Au one. In previous work, Simões et al. [1] also obtained the same onset potential for the electrooxydation of glycerol on Pd/C and Au/C monometallic catalysts prepared by water in oil microemulsion. According to Beden et al [30] the formation of a sub-monolayer of adsorbed hydroxyl groups (required for the oxidation of an primary alcohol to either $CO_3^{2-}$ or $R\text{-}COO^-$ in alkaline medium) at the gold surface is favored in alkaline medium at rather low potentials; it may also that the small size of the gold nanoparticles obtained by plasma sputtering [31] increases the catalytic activity of the material. Pure gold catalyst is active over a broad range of potentials from 0.6 to 1.3 *vs* RHE whereas the pure palladium catalyst is characterized by a narrow potential range of activity from ca. 0.6 V to ca. 1.0 V *vs* RHE. The wet chemistry $Pd_{0.7}Au_{0.3}$ catalyst displays activity a little bit higher than the sputtered Pd and Au catalysts for potentials lower than ca. 0.7 V. Bimetallic co-sputtered $Pd_{0.7}Au_{0.3}$ catalyst presents a shift of the onset potential of ca. 0.1 V toward lower potentials than that obtained with Pd and Au catalysts. The addition of small

amount of gold in the Pd catalyst led to an increase of the catalytic activity from ca. 0.5 to 0.8V *vs* RHE. The current density achieved at 0.65 V vs RHE in Figures 6a and b with the co-sputtered $Pd_{0.7}Au_{0.3}$ catalyst is about 10 times higher than that recorded with the pure palladium and gold catalysts. It has to be noted that the mass activity of the catalyst prepared by plasma sputtering is much higher than that obtained with the catalyst prepared by wet chemistry, as the metal loading is twice lower. Concerning the sputtered catalysts, the total metal loadings measured by RBS are always ca. 70 $\mu g.cm^{-2}$, so that it has no influence on the activity change.

The electrocatalytic activity of the $Pd_{0.7}Au_{0.3}$ catalyst is compared with those obtained with the alternate-sputtered $Pd_{0.35}Au_{0.3}Pd_{0.35}$ and $Au_{0.15}Pd_{0.7}Au_{0.15}$ in Figure 6b. All considered catalysts have same overall $Pd_{0.7}Au_{0.3}$ bulk atomic composition determined by EDX (Table 1) and same metal loading (ca. 70 $\mu g\ cm^{-2}$) determined by RBS. Again, the co-sputtered $Pd_{0.7}Au_{0.3}$ material displays the highest catalytic activity toward glycerol electrooxydation. The following order for the electrocatalytic activity at 0.65 V is obtained: co-sputtered $Pd_{0.7}Au_{0.3}$ ~ sputtered $Au_{0.15}Pd_{0.3}Au_{0.15}$ > wet chemistry $Pd_{0.7}Au_{0.3}$ > sputtered $Pd_{0.35}Au_{0.15}Pd_{0.35}$ > sputtered Pd > sputtered Au.

It is interesting to remark that the co-sputtered $Pd_{0.7}Au_{0.3}$ and the alternate sputtered $Pd_{0.35}Au_{0.15}Pd_{0.35}$ materials display about the same surface atomic composition of alloyed PdAu, being close to ca. 80 at% of Pd and 20 at% of Au. However, their catalytic activity are very different, the co-sputtered catalyst being more active that the alternate sputtered one from ca. 0.5 to 0.8 V. In contrary, co-sputtered $Pd_{0.7}Au_{0.3}$ and alternate sputtered $Au_{0.15}Pd_{0.3}Au_{0.15}$ catalysts have different surface alloy composition and almost the same activity for potential lower than 0.8 V. The cyclic voltammograms in Figure 5 indicate that the active surface area must be of the same order for both catalysts as the oxide reduction peaks have about the same intensities and surface. So it seems that the composition of the

PdAu surface alloy is not the only parameter leading to catalytic improvement toward glycerol electrooxidation. It is worth to note that the most active catalysts were those exhibiting non alloyed gold sites to their surface, as it was revealed by cyclic voltammograms in supporting electrolyte (Figure 5) with the reduction peaks at ca. 1.04 V, and confirmed by the curves in Figure 6b where a second glycerol oxidation peak at potential higher than 1.0 V is visible on the co-sputtered $Pd_{0.7}Au_{0.3}$ and alternate sputtered $Au_{0.15}Pd_{0.7}Au_{0.15}$ catalysts. Simoes et al. obtained their best performance toward glycerol oxidation with a $Pd_{0.3}Au_{0.7}$/C catalyst (31 at% Pd and 69 at% Au determined by ICP-OES) giving a surface alloy composition of 61 at% Pd and 39 at% Au and showing a marked gold oxide reduction peak at ca. 1.04 V [1].

Looking at the j-E curves recorded at Pd and Au catalysts in Figure 6a, both materials lead to the same onset potential for the glycerol oxidation close to 0.6 V *vs* RHE. In a first rapid glance, it could then be concluded that the attribution of the catalytic improvement with PdAu alloys to a bifunctional mechanism [32], where the catalytic metal (palladium) adsorbs alcohol species and the foreign metal (gold) brings adsorbed OH species at lower potentials to complete the oxidation reactions into products, is not adapted to the PdAu systems. However, Beden et al. showed that in alkaline medium oxygenated species could adsorb on gold surface from potentials as low as 0.4 V [30]. Adžić and Avramoc-Ivić [33] studied the oxidation reaction of ethylene glycol in alkaline medium on Au (111), Au (110) et Au (100) surfaces; they proposed that the hydroxyl ions adsorption with a partial charge transfer toward the gold surface, according to equation (9), could be the determining step for alcohol oxidation.

$$Au + OH^- \rightarrow AuOH_{ads}^{\lambda} + (1-\lambda)e^- \qquad (9)$$

Moreover, they showed that this reaction was surface structure sensitive. The adsorption of hydroxyl ions on gold single crystals occurred at lower potential according to the following

order: Au (110), Au (100) et Au (111). They verified that the onset potential of ethylene glycol oxidation in alkaline medium followed the same order as that obtained for the hydroxyl ion adsorption on gold. Avramov-Ivić et al. [34] confirmed that the determining step for glycerol oxidation on a Au(100) surface was the partial adsorption of hydroxyl ions at the surface. Moreover, they proposed that the first step of glycerol oxidation on Au(100) was the interaction between the hydrogen atom bounded to the carbon bearing the secondary alcohol group, with $AuOH_{ads}$ –like species. Moreover, these authors also proposed that glycerol is not adsorbed on gold before the formation of the $AuOH_{ads}$ surface structure.

It seems then that interaction of non alloyed gold sites with alloyed PdAu or with Pd sites allows enhancing the catalytic activity of PdAu materials. Such behavior was already proposed by Brankovic et al. [35] and by Dubau et al. [36,37] for the electrooxidation of methanol and carbon monoxide on PtRu catalysts. These authors showed that non alloyed Pt-Ru catalysts displayed higher catalytic activity. Petrii et al. [38,39] studied the electrooxidation of alcohols containing more than one carbon atom and the effect of adatoms on platinum. They conclude that the presence of adatoms leads to significant effect on the amount and course of electro-oxidation of strongly bonded species and that it is also possible that they affect the composition of chemisorbed species. In agreement with the bi-functional mechanism, the considerable electrocatalytic activity effect of adatoms in the electrooxidation of glycerol may be explained assuming their oxygen adsorbing character, notably $OH_{ads}$. Our results are in agreement with these propositions, the oxygen adsorbing character of Au leading to the decrease of the onset potential of glycerol electrooxidation, and the effect on the amount and course of electro oxidation of strongly adsorbed species on palladium may explain the difference in catalytic activity.

## 4. Conclusion

Platinum-free nano-catalysts have been synthesized by different plasma sputtering processes. PdAu nano catalysts with deferent structure have been characterized and their activity toward the glycerol electro-oxidation has been investigated by cyclic voltammetry. The surface of co-sputtered $Pd_{0.7}Au_{0.3}$ and alternate sputtered $Pd_{0.35}Au_{0.3}Pd_{0.35}$ and $Au_{0.15}Pd_{0.7}Au_{0.35}$ materials are partly composed by PdAu alloy. Several new insights on the synergetic effect between Pd and Au were pointed out:

- plasma sputtering method leads to more active bimetallic PdAu material than wet chemistry method, due to electrode structure and surface composition;

- the modification of palladium by gold leads to increase the catalytic activity toward glycerol electrooxidation;

- the PdAu surface alloy composition has no significant effect on the catalytic activity;

- the presence of non-alloyed gold sites on the material surface leads to the enhancement of the catalytic activity;

- the mechanism seems to involve glycerol adsorption on palladium surface and hydroxyl species formation on gold surface leading to catalytic activity enhancement through the bifunctional mechanism.

Non alloyed Pd+Au catalyst with structure resembling that of non-alloyed Pt+Ru catalyst developed by Dubau et al. [36,37] could be the best one for glycerol oxidation in alkaline medium.

## Acknowledgements

This work was carried out under the framework of a project (AMELI-0Pt) from the ‘‘Programme Interdisciplinaire Energie’’ of CNRS (French National Center for Scientific

Research). B. Courtois and T. Sauvage (CEMHTI, Orléans) are acknowledged for RBS measurements.

| | Pd | Au | $Pd_{0.7}Au_{0.3}$ | $Pd_{0.35}Au_{0.3}Pd_{0.35}$ | $Au_{0.15}Pd_{0.7}Au_{0.15}$ |
|---|---|---|---|---|---|
| Plasma sputtering experimental condition | | | | | |
| $U_{Pd}/U_{Au}$ (V) | -300/0 | 0/-250 | -245/-175 | -250/0 ; 0/-250 ; -250/0 | 0/-250/0 ; -250/0 ; 0/-250 |
| t (min) | 10 | 7.5 | 7.33 | 3.5 / 4.66 / 3.5 | 2.33 / 7 /2.33 |
| P (W) | 193 | 145 | 185 | 135 | 145 |
| Characterization of materials | | | | | |
| Loading (µg $cm^{-2}$) | 75 | 71 | 66 | 62 | 72 |
| Bulk Pd/Au at% by EDX | 100/0 | 0/100 | 66/34 | 70/30 | 70/30 |
| Surface alloy comp. Pd/Au at% | 100/0 | 0/100 | 80/20 | 77/23 | 69/31 |

**Table 1: Configuration of the parameters for the plasma sputtering of Pd and Au atoms and characterization data relative to the synthesized plasma PdAu materials.**

| | $Q_{red}^{PdO}$ / mC | $Q_{red}^{AuO}$ / mC | $Q_{red}^{Pd-Au(O)}$ / mC | $S_{Pd}$ / $cm_{Pd}^2$ | $S_{Au}$ / $cm_{Au}^2$ | $S_{Pd-Au}$ / $cm_{PdAu}^2$ | $S_{total}$ / $cm_{metal}^2$ |
|---|---|---|---|---|---|---|---|
| **Co-sputtered $Pd_{0.7}Au_{0.3}$** | **-** | **0.063** | **0.71** | **-** | **0.16** | **1.70** | **1.86** |
| **wet chemistry $Pd_{0.7}Au_{0.3}$** | **-** | **-** | **1.21** | **-** | **-** | **2.87** | **2.87** |
| **Sputtered $Pd_{0.35}Au_{0.3}Pd_{0.35}$** | **0.42*** | **-** | **0.82*** | **1.05** | **-** | **1.97** | **3.02** |
| **Sputtered $Au_{0.15}Pd_{0.7}Au_{0.15}$** | **-** | **0.07** | **0.64** | **-** | **0.19** | **1.53** | **1.72** |

**Table 2: determination of the charge involved in the reduction peaks of the different metallic phases in the PdAu bimetallic materials, of the related real surface for each phase and of the total real metal surface represented by the sum of the real surfaces of each phase.**

**For the $Pd_{0.35}Au_{0.3}Pd_{0.3}$ where clearly the Pd oxide reduction peak and the PdAu alloy oxide reduction peak partially superimposed, two Gaussian function were used to fit the reduction curve.**

**Figure caption**

Figure 1: RBS spectrum obtained for the co-sputtered $Pd_{0.7}Au_{0.3}$, the 3-layer alternate sputtered $Pd_{0.35}Au_{0.3}Pd_{0.35}$ and $Au_{0.15}Pd_{0.7}Au_{0.15}$ materials.

Figure 2: SEM micrograph obtained for (a) the co-sputtered $Pd_{0.7}Au_{0.3}$ material and (b) the 3-layer alternate sputtered $Pd_{0.35}Au_{0.3}Pd_{0.35}$ material.

Figure 3: Cyclic voltammograms of (**—**) sputtered Pd catalyst and of (—) sputtered Au catalyst.
($v = 50$ mV $s^{-1}$, $N_2$-saturated 1.0 M NaOH electrolyte, T = 293 K).

Figure 4: TEM pictures and related particle size distribution of (a) Pd/C and (b) Au/C materials.

Figure 5: Cyclic voltammograms of the co-sputtered $Pd_{0.7}Au_{0.3}$ catalyst, and of the 3-layer alternate sputtered $Pd_{0.35}Au_{0.3}Pd_{0.35}$ and $Au_{0.15}Pd_{0.7}Au_{0.15}$ catalysts.
($v = 50$ mV $s^{-1}$, $N_2$-saturated 1.0 M NaOH electrolyte, T = 293 K).

Figure 6: Polarization curves of glycerol oxidation recorded (a) on sputtered Pd1 and Au1, co-sputtered $Pd_{0.7}Au_{0.3}$ and wet chemistry $Pd_{0.7}Au_{0.3}$/C catalysts, and (b) on co-sputtered $Pd_{0.7}Au_{0.3}$, wet chemistry $Pd_{0.7}Au_{0.3}$/C, and alternate sputtered $Pd_{0.35}Au_{0.3}Pd_{0.35}$ and $Au_{0.15}Pd_{0.3}Au_{0.15}$ catalysts.
($v = 10$ mV $s^{-1}$, $N_2$-saturated, 0.1 M glycerol + 1.0 M NaOH electrolyte, T = 293 K).

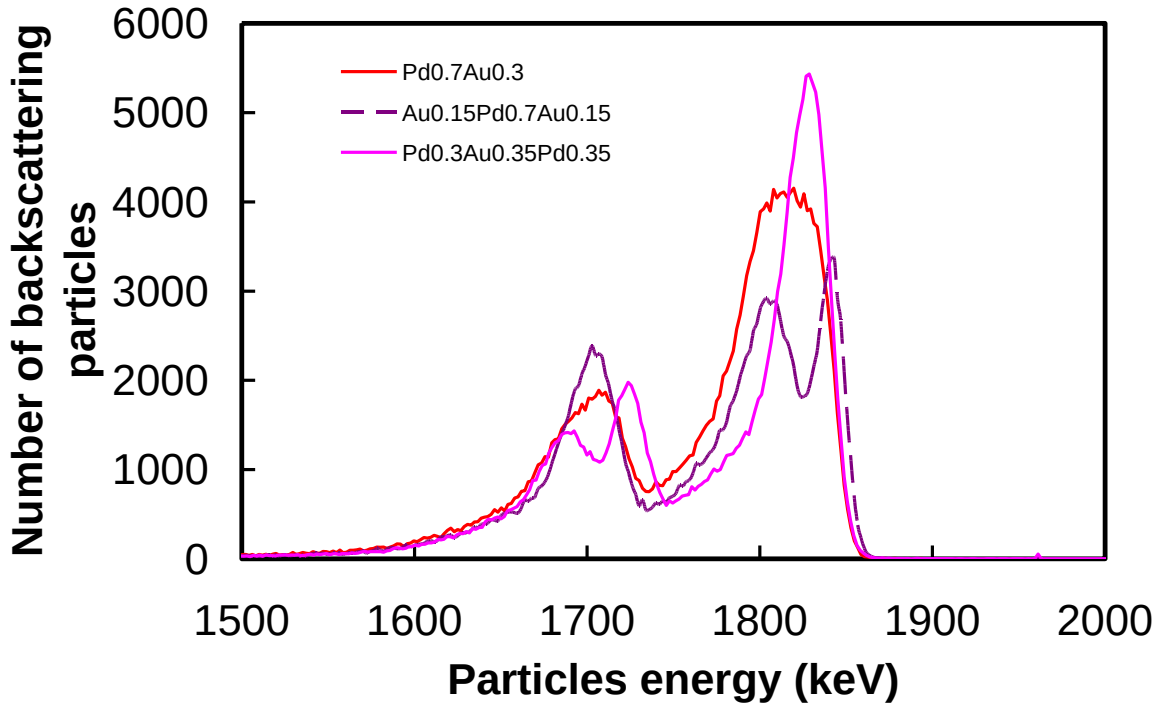


Figure 1

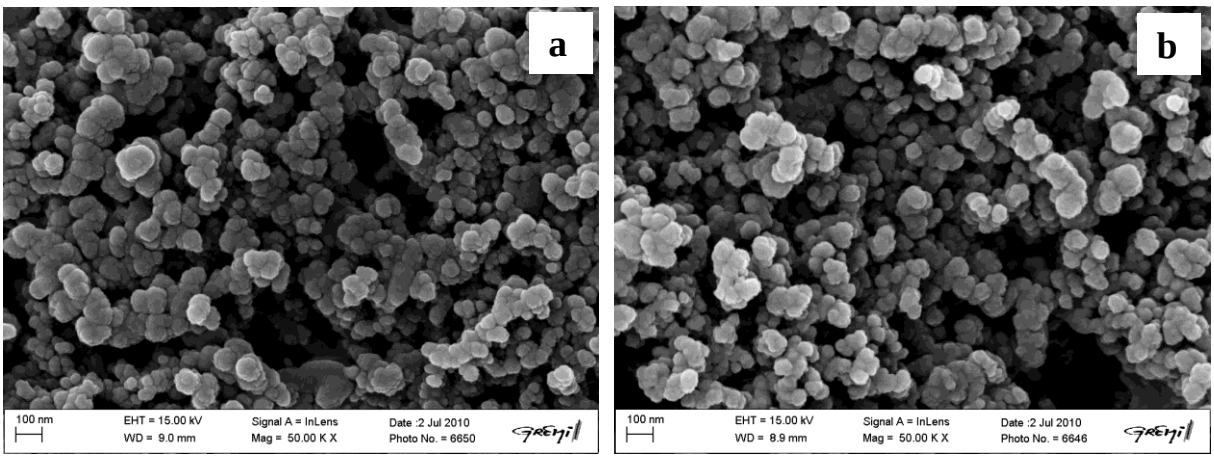


Figure 2

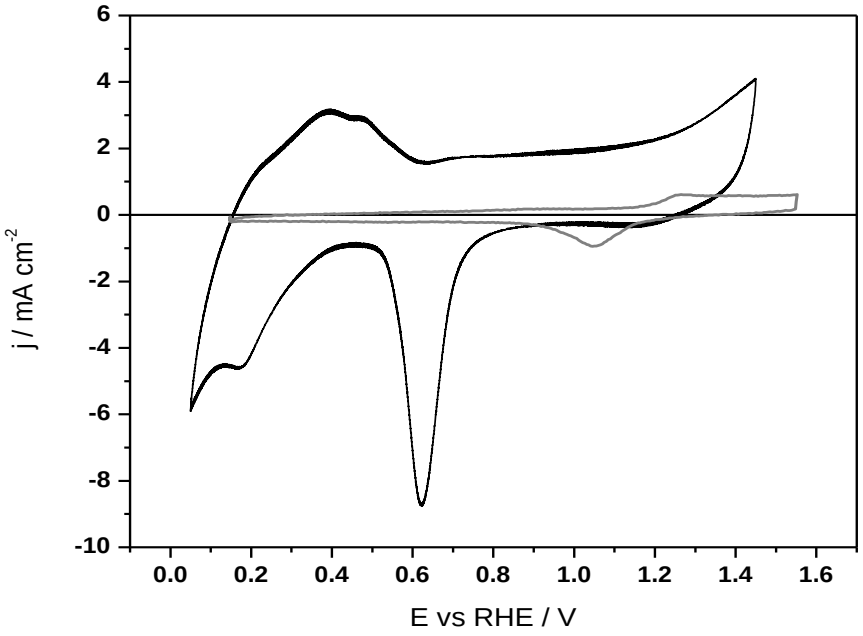


Figure 3

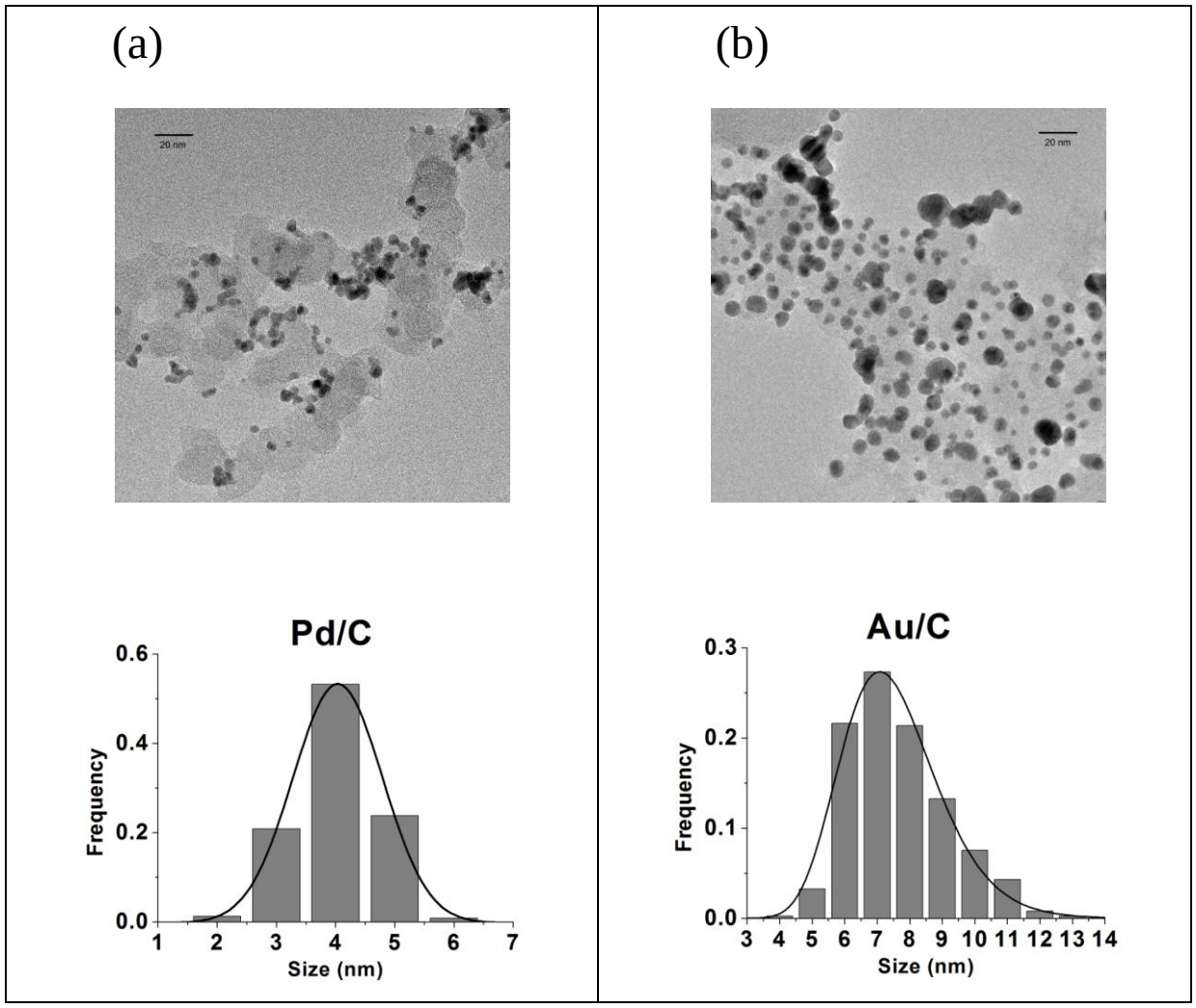
(a)
(b)
20 nm
20 nm
Pd/C
Au/C
Frequency
Size (nm)
0.0
0.2
0.4
0.6
0.1
0.3
1 2 3 4 5 6 7
3 4 5 6 7 8 9 10 11 12 13 14

Figure 4

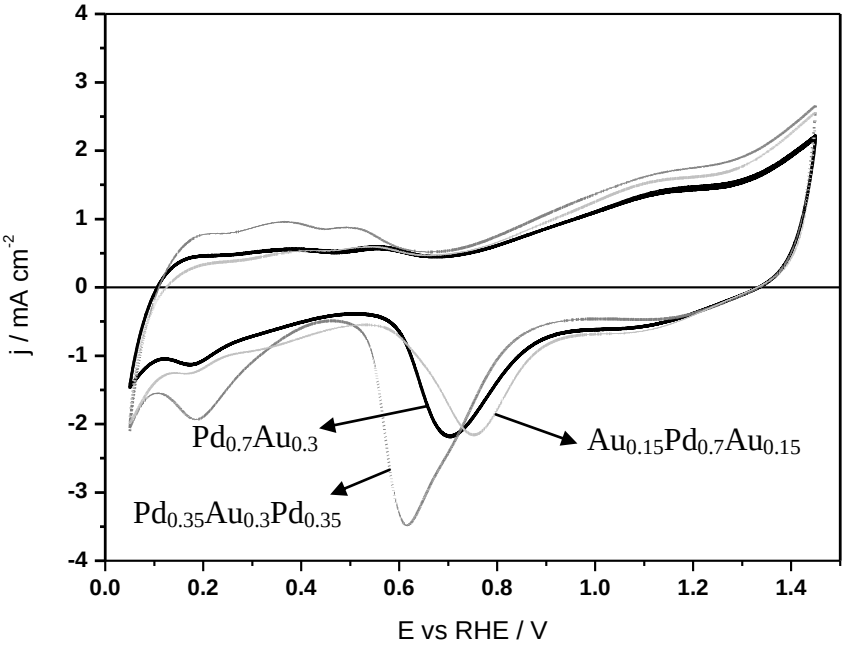
4
3
2
1
0
-1
-2
-3
-4
0.0
0.2
0.4
0.6
0.8
1.0
1.2
1.4
j / mA cm-2
E vs RHE / V
Pd0.7Au0.3
Au0.15Pd0.7Au0.15
Pd0.35Au0.3Pd0.35

Figure 5

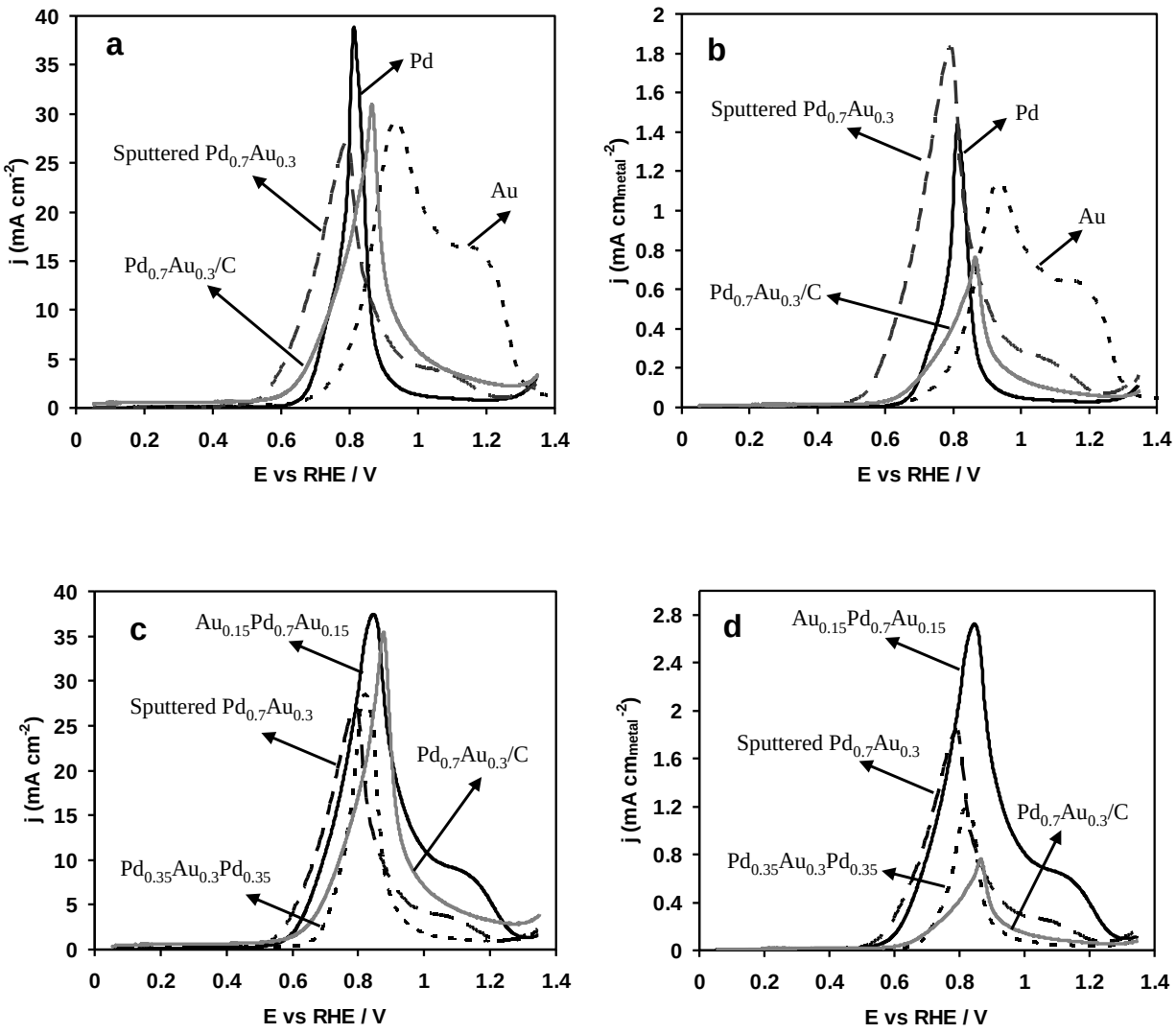
a
Pd
Sputtered Pd0.7Au0.3
Au
Pd0.7Au0.3/C
j (mA cm-2)
E vs RHE / V
b
Sputtered Pd0.7Au0.3
Pd
Au
Pd0.7Au0.3/C
j (mA cmmetal-2)
E vs RHE / V
c
Au0.15Pd0.7Au0.15
Sputtered Pd0.7Au0.3
Pd0.7Au0.3/C
Pd0.35Au0.3Pd0.35
j (mA cm-2)
E vs RHE / V
d
Au0.15Pd0.7Au0.15
Sputtered Pd0.7Au0.3
Pd0.7Au0.3/C
Pd0.35Au0.3Pd0.35
j (mA cmmetal-2)
E vs RHE / V

Figure 6

**Références**


1- M. Simoes, S. Baranton, C. Coutanceau, Appl. Cata. B : environmental 93 (2010) 354-362.

2- S. S. Yazadani, R. Gonzalez, Curr. Opin. Biotechnol. 18 (2007) 213.

3- M. A. Dasari, P. P. Kiatsimkul, W. R. Sutterlin, G. J. Suppes, Appl. Catal. A: Gen. 281 (2005) 225.

4- J.-M. Clacens, Y. Pouilloux, J. Barrault, J. Appl. Catal. A: Gen. 227 (2002) 181.

5- C. Lamy, J.-M. Léger, J. Phys. IV 4 (1994) C1.

6- F. Vigier, C. Coutanceau, A. Perrard, E.M. Belgsir, C. Lamy, J. Appl. Electrochem. 34 (2004) 439.

7- C. Coutanceau, L. Demarconnay, J.-M. Léger, C. Lamy, J. Power Sources 156 (2006) 14.

8- C. Bianchini, P.K. Shen, Chem. Rev. 109 (2009) 4183.

9- D. Z. Jefferery, G. A. Camara, Electrochem. Comm. 12 (2010) 1129.

10- A. Caillard, C. Coutanceau, P. Brault, J. Mathias, J.-M. Léger, J. Power Sources, 162 (2006) 66.

11- M. Mougenot, A. caillard, P. Brault, S. baranton, C. Coutanceau, Int. J. Hyd. En. (2011) doi:10.1016/j.ijhydene.

12- P. Andreazza, C. Andreazza-Vignolle, J. P. Rozenbaum, A. -L. Thomann, P. Brault, Surf. Coat. Tech. 151 (2002) 122.

13- A. L. Thomann, P. Brault, J. P. Rozenbaum, C. Andreazza-Vignolle, P. Andreazza, H. Estrade-Szwarckopf, B. Rousseau, D. Babonneau, G. Blondiaux, J. Phys. D: Appl. Phys. 30 (1997) 3197.

14- P. Brault, A. Caillard, A.-L. Thomann, J. Mathias, C. Charles, R.W. Boswell, S. Escribano, J. Durand,T. Sauvage, J. Phys. D: Appl. Phys. 37 (2004) 3419.

15- A. Caillard, C. Charles, R. Boswell, P. Brault, C. Coutanceau, Appl. Phys. Lett. 90 (2007) 223119.

16- M. Cavarroc, A. Ennadjaoui, M. Mougenot, P. Brault, R. Escalier, Y. Tessier, J. Durand, S. Roualdès, T. Sauvage, C. Coutanceau, Electrochem. Comm. 11 (2009) 859.

17- A. Chen, P. Holt-Hindle, Chem. Rev. 110 (2010) 3767.

18- Mário Simões, Stève Baranton, Christophe Coutanceau, J. Phys. Chem. C 113 (2009) 13369.

19- M. Simões, S. Baranton, C. Coutanceau, Electrochim. Acta 56 (2010) 580.

20- F. Gloaguen, N. Andolfatto, R. Durand, P. Ozil, J. Appl. Electrochem. 24 (1994) 863.

21- A. Caillard, P. Brault,T, J. Mathias, C. Charles, R.W. Boswell, T. Sauvage, Surf. Coat. Technol. 200 (2005) 391.

22- M. Grdén, M. Lukaszewski, G. Jerkiewicz, A. Czerwinski, Electrochim. Acta 53 (2008) 7583.

23- A. Habrioux, E. Sibert, K. Servat, W. Voguel, K. B. Kokoh, N. Alonso-Vante, J. Phys. Chem. B 111 (2007) 10329.

24- R. Woods, in: A.J. Bard (Ed.), Electroanalytical Chemistry, vol. 9, Marcel Dekker, New York, 1976, p. 2.

25- A. N. Kahyaoglu, Ph.D. Thesis, University of Poitiers, Poitiers, France, 1981.

26 R. Séllin, J. -M. Clacens, C. Coutanceau, Carbon 48 (2010) 2244.

27 P. Brault, C. Josserand, J.-M. Bauchire, A. Caillard, C. Charles, R. W. Boswell, Phys. Rev. Lett. 102 (2009) 045901.

28- A. J. Rand, R. J. Woods, Electroanal. Chem. 36 (1972) 57.

29 M. Łukaszewski, A. Czerwiński, Thin Solid Films 518 (2010) 3680.

30- B. Beden, A. Cetin, A. Kahyaoglu, D. Takky, C. Lamy, J. Catal. 104 (1987) 37.

31- Gabriel M. Veith, Andrew R. Lupini, Stephen J. Pennycook, GaryW. Ownby, Nancy J. Dudney, Catalysis Today 122 (2007) 248–253.

32- M. Watanabe and S. Motoo, J. Electroanal. Chem. 60 (1975) 2675.

33- R. Adžić, M. Avramoc-Ivić, J. Catal. 101 (1986) 532.

34- M. Avramov-Ivić, J.-M. Léger, C. Lamy, V. Jović, S. Petrović, J. Electroanal. Chem. 308 (1991) 309.

35- S. R. Brankovic, N. S. Marinkovic, J. X. Wang, R. R. Adzic J. Electroanal. Chem. 532 (2002) 57-66.

36- L. Dubau, C. Coutanceau, E. Garnier, J. -M. Léger, C. Lamy, J. Appl. Electrochem. 33 (2003) 419-429.

37- L. Dubau, F. Hahn, C. Coutanceau, J. -M. Léger, C. Lamy, J. Electroanal. Chem. 554-555 (2003) 407-415.

38- B.I. Podlovchenko, O.A. Petrii, A.N. Frumkin, H. Lal, J. Electronal. Chem. 11 (1966) 12.

39- N.W. Smirnova, O.A. Petrii, A. Grzejdziak, J. Electroanal. Chem. 251 (1988) 73.